

P³LS: Point Process Partial Least Squares

Jamshid Namdari*, Robert T. Krafty, Amita Manatunga

Department of Biostatistics & Bioinformatics, Emory University, Atlanta, GA, United States

E-mail: jamshid.namdari@emory.edu

SUMMARY

Many studies collect data that can be considered as a realization of a point process. Included are medical imaging data where photon counts are recorded by a gamma camera from patients being injected with a gamma emitting tracer. It is of interest to develop analytic methods that can help with diagnosis as well as in the training of inexpert radiologists. Partial least squares (PLS) is a popular analytic approach that combines features from linear modeling as well as dimension reduction to provide parsimonious prediction and classification. However, existing PLS methodologies do not include the analysis of point process predictors. In this article, we introduce point process PLS (P^3LS) for analyzing latent time-varying intensity functions from collections of inhomogeneous point processes. A novel estimation procedure for P^3LS is developed that utilizes the properties of log-Gaussian Cox processes, and its empirical properties are examined in simulation studies. The method is used to analyze kidney functionality in patients with renal disease in order to aid in the diagnosis of kidney obstruction.

Key words: Partial least squares; Point process; Log Gaussian Cox process; Functional linear model;

*To whom correspondence should be addressed.

Dimension reduction.

1. INTRODUCTION

Partial Least Squares (PLS), originally proposed by [Wold \(1966\)](#), has emerged as a promising strategy for predicting a response in terms of a covariate. Under linear regression, the classical PLS approach targets on maximizing predictive power while achieving dimension reduction in a supervised manner to extract a set of orthogonal latent factors from predictors. The method has found popularity in chemometrics, in particular, as well as in many other scientific fields including econometrics, bioinformatics, food research, medicine, pharmacology, social sciences, physiology, and industrial and management research. To make PLS applicable to various data types, such as multilevel data and functional data, extensions of the method have been developed. For more on the developments and applications in scientific fields refer to [Rosipal and Krämer \(2005\)](#), [Abdi \(2010\)](#), and [Krishnan *and others* \(2011\)](#). Notably, recent technological advancements have enabled the generation of more complex data structures, which could significantly influence outcomes in scientific research. For instance, in imaging studies, covariates of interest may sometimes be modeled as a realization of a point process. To the best of our knowledge, PLS's extension to incorporate temporal point processes has not been explored.

Point process data is a realization of a random set of points in a specified space such as time, plane, or more complexed spaces. In particular, temporal point process data can be considered as observed times of occurrence of an event of interest, such as times of detection of a gamma photon by a gamma camera or arrival times of a patient to an emergency room. For instance, in our motivating study described in [Section 2](#), details an experiment where the point process of photon counts data are collected over time to aid in the interpretation of kidney obstruction for radiologists. Radionuclide imaging begins with a 24 minute acquisition following the intravenous administration of a gamma-emitting tracer, ^{99m}Tc -mercaptoacetyltriglycine (MAG3), which is

extracted from the blood by the kidneys and drains via the ureters to the bladder. As MAG3 passes through the kidneys, its gamma emissions are captured by a gamma camera for further analysis. To assist in diagnosing kidney obstruction, a region of interest is placed over each kidney and curves are generated by continuously measuring MAG3 photon counts within each kidney. The curves, known as the baseline renogram curve, track the MAG3 photon counts at 59 time points over the 24-minute period. A second curve, termed the post-furosemide renogram, is recorded at 40 time points during an additional 20-minute period following an injection of furosemide, a diuretic that helps to enhance kidney drainage for improved analysis. The physicians interpreting the scans review a sequence of 2-minute images along with the renogram curves and provides a score for each kidney, ranging from -1 to 1, where the values close to 1 indicates the high confidence of kidney obstruction (we refer to as degree of obstruction) whereas a score of -1 indicates high confidence that the kidney is not obstructed. Figure (1) displays the plot of photon counts over the scanning period for four patients. One area of scientific interest has been the development of analytical tools to assist radiologists in interpreting MAG3 scans for suspected kidney obstruction, as well as using these tools to train inexperienced radiologists. To handle the predictor, which involves renogram curves consisting of photon counts over time and its relation to the response of kidney obstruction, various approaches have been proposed with different data settings. These include intuitive methods based on calculating curve characteristics and modeling, latent class modeling, heuristic approaches etc., ([Chang and others, 2020](#); [Taylor and others, 2008](#); [Bao and others, 2011](#)). However, all these approaches treat the photon counts as the observed values without considering the underlying nature of the realization of the point process. Not accounting for full stochastic characteristics of the data as point processes could yield suboptimal inference.

Towards the goal of fitting an interpretable predictive model for predicting severity of obstruction status based on the renogram point process data, we introduce an extension of the

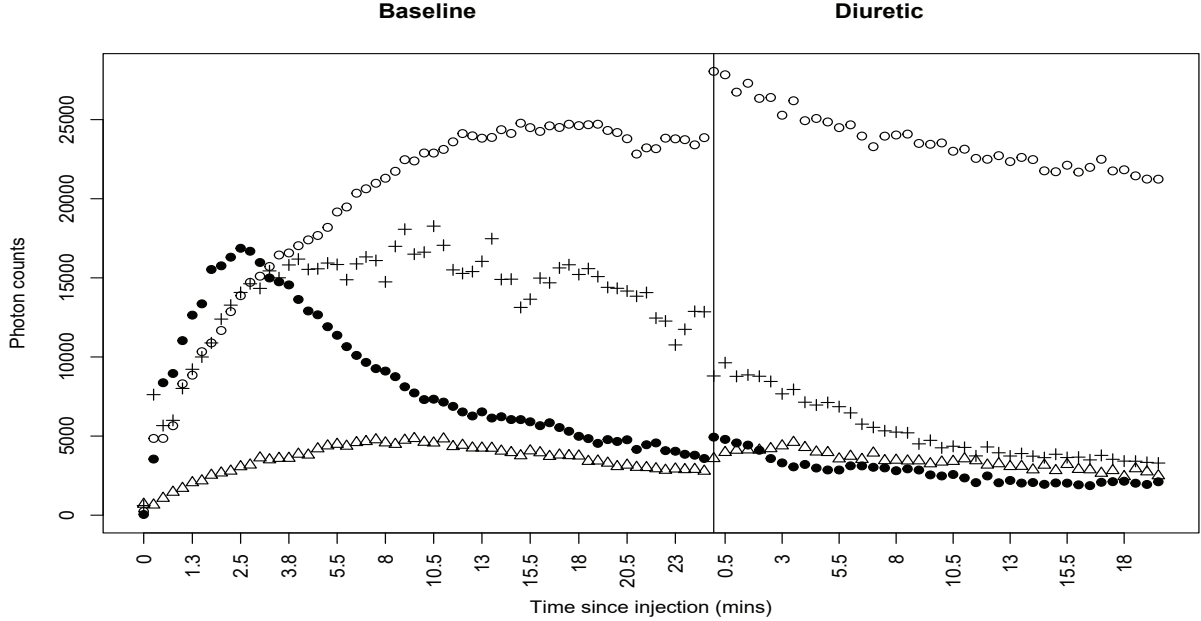


Fig. 1: **Left panel** First scan (Baseline photon counts) during the 24-min scanning period after intravenous injection of (Tc-99mMAG3); **Right panel**: Second scan (Diuretic) for an additional 20-min after intravenous injection of furosemide; with experts' ratings **Solid dots** -0.9, **Plus sign** -0.9, **Triangle** -0.5, **circle** 0.3.

functional PLS of [Delaigle and Hall \(2012\)](#) to point process data. To establish a functional linear relationship between the predictors, which are log-intensity functions of the underlying point processes, and the response, which reflects radiologist's assessment of the degree of obstruction, our approach selects basis functions adaptively to maximize the predictive power of the linear model. In contrast, the common approach of representing functions involves a pre-selected set of basis functions ([Ramsay and Silverman, 2005](#)). Our result yields a more interpretable model that is parsimoniously optimal. Two key challenges in fitting such models, where latent log-intensity functions are not directly observed, are (1) the estimation of the covariance function of the generating log-intensity process, which is necessary for the estimation of the parsimonious basis, and (2) the prediction of individual log-intensities within the parsimonious basis, which are necessary for estimating the coefficient quantifying the association between log-intensities and the outcome.

This article develops a novel procedure that utilizes the properties of the log Gaussian Cox process (Møller *and others*, 1998) to construct efficient estimators of these functional quantities, and represents the first extension of PLS to incorporate log Gaussian Cox point process predictors.

This paper is organized as follows. Section 2 contains a detailed description of the renal study that motivated our methodological development. In Section 3 we describe our approach to point process partial least squares. To illustrate the performance of the proposed methodology, we present a simulation study in Section 4. In addition, in Section 4, we compare the predictive performance of our proposed method to two alternative approaches based on functional principal component regression and partial least squares. Results of the application of the *P³LS* to the renal study is provided in Section 5. We conclude this paper, in Section 6, by a discussion of the limitations and strengths of the proposed method and possible directions of further work related to point process partial least square.

2. MOTIVATING STUDY

The methodology developed in this paper is motivated by a renal study conducted to develop an analytic tool for predicting the presence of obstruction based on a patient's renogram data. An obstructed kidney will irreversibly lose function if the obstruction is not relieved. A widely used approach for evaluating suspected obstruction is radionuclide imaging. Imaging is performed following an intravenous injection of the gamma emitting tracer, technetium-99m mercaptoacetyl-triglycine (Tc-99mMAG3), with additional imaging following the subsequent intravenous administration of a potent diuretic (O'Reilly *and others*, 1996). Lack of opportunity and insufficient training, however, can result in scan interpretations by less experienced radiologists that disagree considerably with each other and disagree with the experts' interpretations (Jaksić *and others*, 2005; Taylor *and others*, 2008, 2012). There is a need for analytic tools to help determine when a kidney is obstructed. Such tools can assist in patient care and in the training of radiology

residents. Successful computerized tools should reduce both intra- and inter-observer variability in MAG3 scan interpretation, and lead to a higher level of performance and standardization.

We consider data from $n = 131$ patients during the period of March 1998 to July 2017 who were referred to the Emory University Hospital with suspected kidney obstruction. Each subject underwent two scans. A first scan called “Baseline” and a second scan following an injection of furosemide, a diuretic, “Diuretic”. The Baseline scan was performed following the intravenous injection of MAG3, which is rapidly removed from the blood by the kidneys and then travels down the ureters from the kidney to the bladder. Photons emitted by the tracer are imaged by a gamma camera/computer system and quantified for analysis by placing a region of interest (ROI) over each kidney. The renogram (time activity) curves are derived from the photon counts detected in the whole kidney ROIs during the 24-min scanning period. Then, the second scan (Diuretic) is obtained after the intravenous injection of furosemide for additional 20 min using a framing rate of 30 sec/frame. In this study, there is no established gold standard for assessing kidney obstruction. Therefore, an expert with extensive knowledge of kidney function and over 25 years of experience in academic nuclear medicine was asked to interpret each kidney’s condition on a scale from -1 to 1, where values approaching 1 indicate a high degree of obstruction. See Figure 1 for renogram curves (Baseline and Diuretic curve) for four subjects with their corresponding obstruction rating scores. When there is high likelihood of kidney obstruction, the baseline curve gradually and steadily increases, while the diuretic curve shows a slow decline from a higher level (eg., circle). In contrast, non-obstructed kidneys exhibit a rapid increase immediately after injection, followed by an early decrease (eg., solid dots).

We have three goals in mind in conducting this analysis. First, we desire to develop a predictive model that predicts a clinical score based on a pair of renal scans, the baseline and diuretic. Second, we desire to obtain latent factors that reveal modes of variation in the data, which is an optimal component of the predictive model. Third, we desire to quantify the association between

log-intensity function and clinical scores.

3. METHODOLOGY

The data considered here are n independent pairs $(\Phi_1, Y_1), \dots, (\Phi_n, Y_n)$, where Y_1, \dots, Y_n are the outcomes (scalar), e.g. experts rating scores, and Φ_1, \dots, Φ_n are realizations of the point process described below. We seek to build a predictive model that can predict Y_i 's using features in the Φ_i 's that parsimoniously represent the dynamics of the point processes. This is achieved by modeling Y_i 's through a linear model incorporating latent intensity functions, $\lambda_i(\cdot)$, that govern the dynamics of the process $\Phi_i, i = 1, \dots, n$ and applying the partial least squares regression as described below. Note that, the partial least squares method along with the estimation procedure proposed in Section 3.1 will be referred to as *P³LS* in this article. Below we describe our model building and model fitting procedure.

For each kidney, say the i^{th} kidney, $i = 1, \dots, n$, the set of times, since the start of scanning, that gamma photons being detected by a gamma camera, denoted by $\Phi_i = \{S_{i1}, S_{i2}, \dots\} \subset \mathbb{R}$, can be viewed as a random set that is referred to as a point process. The point process Φ_i can be described in terms of the total number of detected photons in an interval B , such as $B = (0, t]$, which we denote by $N_i(B)$. This allows us to study the statistical properties of the point process by modeling the probability distribution of $N_i(\cdot)$ over any measurable subset of the real line. Let \mathcal{I} be the time interval over which kidneys were imaged. In our application this is the union of two continuous intervals, one for the Baseline scan and one for the Diuretic scan. However, \mathcal{I} can be any compact subset of the real line, including a simple continuous interval, or more complicated structures. It is not unreasonable to assume that we can divide \mathcal{I} into small subintervals of length Δ where in each interval $(t, t + \Delta]$ there is a positive probability of detecting at least one photon, but the probability of detecting more than one photon is negligible. In addition, we would like to allow the probability of detecting a gamma photon over Δ to depend on time, in other

words the instantaneous probability of observing one photon at each time point, t , be a function $\lambda_i(t)$ of time. Finally, we assume that emission of photons at time t does not have excitatory or inhibitory effect on emissions of photons at a later time. In other words, we can assume that for two non-overlapping intervals B_1 and B_2 , $N_i(B_1)$ and $N_i(B_2)$ are independent. This suggests considering Poisson distribution for the photon counts in a set B . Note that $\lambda_i(t)$ can be viewed as $\lim_{\Delta \rightarrow 0} E[N_i(t, t + \Delta)]/\Delta$, which indicates the rate at which photons are detected by a gamma camera at time t . Lastly, to account for varying levels of obstruction among kidneys, we assume that $\lambda_i(t)$ is a random function such that $\log[\lambda_i(t)]$ follows a Gaussian process. The point process described above is called log-Gaussian Cox process.

To be more precise, consider the point processes Φ_1, \dots, Φ_n . For each $\Phi_i, i = 1, \dots, n$, let $N_i(B) = \text{card}\{\Phi_i \cap B\}$ be the number of events of Φ_i in a Borel set $B \subset \mathbb{R}$ and define the intensity measure of Φ_i to be $\Lambda_i(B) = E[N_i(B)]$ with the intensity function $\lambda_i(x)$, i.e. $\Lambda_i(B) = \int_B \lambda_i(x) dx$. Φ_i is called a Poisson process on $\mathcal{I} \subset \mathbb{R}$ with intensity measure Λ_i if for any $B \subset \mathcal{I}$ satisfies

- $N_i(B)$ is Poisson distributed with mean $\Lambda_i(B)$,
- conditional on $N_i(B)$, the points in $\Phi_i \cap B$ are iid with density proportional to $\lambda_i(x)$, $x \in B$.

Moreover, Φ_i is called a Cox process driven by a non-negative process λ_i if, conditional on λ_i , Φ_i is a Poisson process with intensity function λ_i . In this paper we consider the log Gaussian Cox Poisson process, introduced by [Møller and others \(1998\)](#), where $\log[\lambda_i(t)] = \log[\lambda_0(t)] + \Xi_i(t)$, and Ξ_i 's are zero-mean independent Gaussian processes with a common covariance function $K(s, t) = \text{Cov}[\Xi_i(s), \Xi_i(t)]$. Suppose Φ_1, \dots, Φ_n be n realizations of a log Gaussian Cox process driven by $\lambda_1, \dots, \lambda_n$, respectively. In this article we denote the log-intensities by $X_i := \log(\lambda_i)$.

To introduce the predictive model, consider the independent pairs $(X_1, Y_1), \dots, (X_n, Y_n)$, where $X_i, i = 1, \dots, n$ are the log-intensity functions defined on the nondegenerate, compact interval \mathcal{I} and satisfying $\int_{\mathcal{I}} E(X_i^2) < \infty$, and Y_1, \dots, Y_n are scalar random variables generated by

the following linear model

$$Y_i = a + \int_{\mathcal{I}} b(t)X_i(t) dt + \epsilon_i, \quad i = 1, \dots, n. \quad (3.1)$$

Here a is a scalar parameter, $\epsilon_i, i = 1, \dots, n$ are iid random variables with finite second moment such that $E(\epsilon_i|X_i) = 0$, and b , a function valued parameter, is a square integrable function on \mathcal{I} . Recall that in our motivating example, \mathcal{I} is the union of continuous intervals for the Baseline and Diuretic scans, but this model and P^3LS methodology applies to any compact subset of the real line \mathcal{I} , including a single continuous interval of time. The class of square integrable functions on \mathcal{I} we considered here, denoted by $\mathcal{C}(\mathcal{I})$, is equipped with the inner product and the norm defined as $\langle u, v \rangle := \int_{\mathcal{I}} u(s)K(s, t)v(t)dsdt$ and $\|u\| := \sqrt{\langle u, u \rangle}$, where $K(s, t) = \text{Cov}[X_i(s), X_i(t)]$, for $u, v \in \mathcal{C}(\mathcal{I})$. Note that, the condition $E(\epsilon_i|X_i) = 0$ implies $a = E(Y_i) - \int_{\mathcal{I}} b(t)E[X_i(t)] dt$, so $Y_i = E(Y_i) + \int_{\mathcal{I}} b(t) \{X_i(t) - E[X_i(t)]\} dt + \epsilon_i$.

To estimate the coefficient function in (3.1), typically one expands X_i 's and b in a system of orthonormal basis functions, $\{\psi_1, \psi_2, \dots\}$, and estimate b by finding optimal coefficients in the truncated expansion, b_p of b , where

$$b_p = \sum_{j=1}^p \beta_j \psi_j, \quad (3.2)$$

and β_1, \dots, β_p are coefficients corresponding to basis functions. Note that, by approximating b with b_p , the truncated form of the linear functional $a + \int_{\mathcal{I}} b(t)X_i(t) dt$ can be written as, say $g_p(X_i)$, where

$$g_p(X_i) := E(Y_i) + \sum_{j=1}^p \beta_j \int_{\mathcal{I}} \{X_i(t) - E[X_i(t)]\} \psi_j(t) dt. \quad (3.3)$$

Then, we can approximate Y_i by $g_p(X_i) + \epsilon_i$ and determine β_1, \dots, β_p through the least squares method, i.e. by minimizing

$$\beta_1, \dots, \beta_p = \arg \min_{w_1, \dots, w_p} \frac{1}{n} \sum_{i=1}^n \left\{ Y_i^c - \sum_{j=1}^p w_j \int_{\mathcal{I}} X_i^c(t) \psi_j(t) dt \right\}^2, \quad (3.4)$$

where $Y_i^c = Y_i - \bar{Y}$, $X_i^c(t) = X_i(t) - \bar{X}(t)$, and $\bar{X}(t) = \sum_{j=1}^n X_j(t)/n$.

One adaptive procedure for selecting the basis functions that captures both the covariance structure of X_i 's as well as the linear relationship between Y_i and X_i is through the Partial Least Squares (PLS) regression. [Delaigle and Hall \(2012\)](#) proposed a functional partial least squares procedure for constructing the basis functions ψ_1, \dots, ψ_p in a sequential manner, such that for $p = 1$, ψ_1 is determined so that $\|\psi_1\| = 1$ and $\text{Cov}\{Y_i - E(Y_i), \int_{\mathcal{I}} [X_i(t) - E(X_i(t))] \psi_1(t) dt\}$ is maximized. Note that, when $p = 1$, $b_1 = \beta_1 \psi_1$ and the linear model (3.1) reduces to simple linear regression model $Y_i = E(Y_i) + \beta_1 \int_{\mathcal{I}} \{X_i(t) - E[X_i(t)]\} \psi_1(t) dt + \epsilon_i$, where β_1 can be determined by the least squares method. Next, the second PLS basis function, ψ_2 , is determined such that it is orthogonal to ψ_1 and the covariance between the deflated response (response after removing the linear effect of ψ_1 on the Y_i) and the projected data onto ψ_2 is maximized, i.e. $\psi_2 = \arg \max_{\psi} \text{Cov}\{Y_i - g_1(X_i), \int_{\mathcal{I}} (X_i(t) - E[X_i(t)]) \psi(t)\}$ such that $\langle \psi_1, \psi_2 \rangle = 0$ and $\|\psi_2\| = 1$, where $g_1(X_i) = E(Y_i) + \beta_1 \int_{\mathcal{I}} \{X_i(t) - E[X_i(t)]\} \psi_1(t) dt$. Sequentially, in the same manner, the p -th PLS basis function is constructed such that the covariance functional

$$f_p(\psi_p) = \text{Cov} \left\{ Y_i - g_{p-1}(X_i), \int_{\mathcal{I}} X_i(t) \psi_p(t) dt \right\}, \quad (3.5)$$

is maximized subject to $\|\psi_p\| = 1$ and $\langle \psi_j, \psi_p \rangle = 0$ for $1 \leq j \leq p-1$, where g_p and b_p are defined in equations (3.3) and (3.2), representing the truncated expansions of the linear functional $a + \int_{\mathcal{I}} b(t) X_i(t) dt$ and the coefficient function b , with respect to ψ_1, \dots, ψ_p , respectively. In addition, for each $p \in \mathbb{N}$, β_1, \dots, β_p are obtained by minimizing the mean squared error of prediction as in (3.4).

An interesting property of the PLS basis functions is that for each $p \geq 1$, the linear representation of any function in ψ_1, \dots, ψ_p is equivalent to representing it as a linear combination of $K(b), \dots, K^p(b)$, where

$$K(b)(t) = \int_{\mathcal{I}} b(s) K(s, t) ds, \quad (3.6)$$

$$K^j(b)(t) = \int_{\mathcal{I}} K^{j-1}(s) K(s, t) ds, \quad j > 1. \quad (3.7)$$

See [Delaigle and Hall \(2012\)](#) for more details. This motivates considering basis functions ψ_1, ψ_2, \dots that are obtained by applying the modified Gram-Schmidt orthonormalization procedure (outlined in the Supplementary Materials) to $K(b), K^2(b), \dots$. We adopt the above procedure for constructing PLS basis functions for the P^3LS procedure in this paper.

In the context of point process data, we note that log-intensity functions, X_1, \dots, X_n , are not observable. That is, we need to estimate $X_j, j = 1, \dots, n$, in addition to the covariance function, $K(s, t)$, using the realizations of the point process that we describe in the next section.

3.1 Estimation Procedure

3.1.1 Estimation of the Covariance Functions We proceed with estimation of the covariance function of the log-intensities by using their relation to the second order intensities, denoted and defined as $\rho_{i,j}^{(2)}(s, t) := E[\lambda_i(s)\lambda_j(t)]$ for $i, j = 1, \dots, n$, accompanied with an application of Campbell's Theorem ([Daley and Vere-Jones, 2003](#)).

Using the moment generating function of the normal distribution

$$E[\lambda_i(s)\lambda_i(t)] = E[\lambda_i(s)]E[\lambda_i(t)] \exp\{K(s, t)\}, \quad \text{for } i = 1, \dots, n. \quad (3.8)$$

Thus,

$$K(s, t) = \log \frac{E[\lambda_i(s)\lambda_i(t)]}{E[\lambda_i(s)]E[\lambda_i(t)]}, \quad \text{for } i = 1, \dots, n. \quad (3.9)$$

In addition, since the n random intensity functions are independent, $E[\lambda_i(s)\lambda_j(t)] = E[\lambda_i(s)]E[\lambda_j(t)]$ for all $i \neq j$ and $E[\lambda_i(t)] = E[\lambda_j(t)]$ for all $i, j = 1, \dots, n$. Thus, we can rewrite (3.9) as

$$K(s, t) = \log \frac{\rho_{i,i}^{(2)}(s, t)}{\rho_{i,j}^{(2)}(s, t)}, \quad \text{for } i, j = 1, \dots, n \text{ and } i \neq j. \quad (3.10)$$

By Campbell's Theorem, for any measurable function, $f(u, v)$

$$E \left[\sum_{u \in \Phi_i} \sum_{v \in \Phi_j}^{u \neq v} f(u, v) \right] = \int \int f(u, v) \rho_{i,j}^{(2)}(u, v) du dv, \quad (3.11)$$

where the expectation is over the point processes Φ_i and Φ_j . By borrowing ideas in [Xu and others \(2020\)](#), we can select $f(u, v) = \kappa_h(s - u)\kappa_h(t - v)/[a(s; h)a(t; h)]$, where $\kappa(\cdot)$ is a kernel function, $\kappa_h(u) = \kappa(u/h)/h$, and $a(s; h) = \int \kappa_h(s - x)dx$ is an edge correction term. Then, we can estimate $K(s, t)$, denoted by $\hat{K}(s, t)$, by the plug in estimator where the numerator, $E[\lambda_i(s)\lambda_i(t)]$, and denominator, $E[\lambda_i(s)]E[\lambda_i(t)]$, of [\(3.9\)](#) are estimated by $E[\widehat{\lambda_i(s)\lambda_i(t)}]$ and $E[\widehat{\lambda_i(s)}]E[\widehat{\lambda_i(t)}]$, respectively, given by

$$E[\widehat{\lambda_i(s)\lambda_i(t)}] = \frac{1}{n} \sum_{i=1}^n \sum_{x \in \Phi_i} \sum_{y \in \Phi_i}^{x \neq y} \frac{\kappa_h(s - x)\kappa_h(t - y)}{a(s; h)a(t; h)}, \quad (3.12)$$

$$E[\widehat{\lambda_i(s)}]E[\widehat{\lambda_i(t)}] = \frac{1}{n(n-1)} \sum_{i,j=1, \dots, n}^{i \neq j} \sum_{x \in \Phi_i} \sum_{y \in \Phi_j}^{x \neq y} \frac{\kappa_h(s - x)\kappa_h(t - y)}{a(s; h)a(t; h)}, \quad (3.13)$$

to obtain

$$\hat{K}(s, t) = \log \frac{E[\widehat{\lambda_i(s)\lambda_i(t)}]}{E[\widehat{\lambda_i(s)}]E[\widehat{\lambda_i(t)}]}. \quad (3.14)$$

3.1.2 Estimation of the Intensity Functions Given the eigen functions ϕ_1, ϕ_2, \dots of the covariance function $K(\cdot, \cdot)$, the log-intensities can be expanded as

$$\log [\lambda_i(t)] = \sum_{\ell} \xi_{i\ell} \phi_{\ell}(t). \quad (3.15)$$

This motivates considering the following method for estimating the scores $\xi_{i\ell}, \ell = 1, 2, \dots$. We first partition the time interval, \mathcal{I} , into bins B_1, \dots, B_b and denote the midpoint of each bin by $\bar{t}_1, \dots, \bar{t}_b$. Let $W_{i\ell}, \ell = 1, \dots, b$ be the number of events in the point process Φ_i falling in B_{ℓ} . Note that, $W_{i\ell} \approx \text{Poisson}[\lambda_i(\bar{t}_{\ell}) | B_{\ell}]$. Thus, $E[W_{i\ell} | B_{\ell}] \approx \lambda_i(\bar{t}_{\ell})$. Therefore, we can consider the following log-linear model

$$\log E[W_{i\ell} | B_{\ell}] = \sum_{\ell} \xi_{i\ell} \phi_{\ell}(\bar{t}_{\ell}). \quad (3.16)$$

Note that, estimates of the eigenfunctions of the covariance function $K(\cdot, \cdot)$ can be obtained from those of $\hat{K}(\cdot, \cdot)$, defined in [\(3.14\)](#). Suppose $\hat{K}(\cdot, \cdot)$ is evaluated on the grid $\mathcal{G} = \{t_1, \dots, t_T\} \star \{t_1, \dots, t_T\}$ and v_1, v_2, \dots be the corresponding eigenvectors of \hat{K} . Then, an estimate of the

eigenfunctions ϕ_1, ϕ_2, \dots evaluated on $\{t_1, \dots, t_T\}$ is $\hat{\phi}_\ell = v_\ell/\Delta$, where $\Delta = (t_T - t_1)/T$. This enables us to estimate the log-intensities by truncating (3.15) to the first q terms, i.e. $X_i^{(q)} = \sum_{\ell=1}^q \xi_{i\ell} \phi_\ell(t)$, and plugging in $\hat{\phi}_\ell$ for ϕ_ℓ and $\hat{\xi}_{i\ell}$, obtained through the log-linear model (3.16), for $\xi_{i\ell}$, for $\ell = 1, \dots, q$. The final estimate for X_i is

$$\hat{X}_i^{(q)} = \sum_{\ell=1}^q \hat{\xi}_{i\ell} \hat{\phi}_\ell(t). \quad (3.17)$$

3.1.3 Estimation of the Coefficient Function b Recall that the coefficient function b can be estimated by truncation to the first p terms of the expansion of b with respect to the basis functions ψ_1, ψ_2, \dots , i.e. $b_p = \sum_{j=1}^p \beta_j \psi_j$. In addition, as described in Section 3, ψ_j 's are obtained by applying the modified Gram-Schmidt algorithm to $K(b), K^2(b), \dots$. Here, we utilize the estimates obtained for X_i 's in (3.17) and $\hat{K}(s, t)$ in (3.14) to estimate ψ_j 's and β_j 's. To this end, first we estimate $K^j(b)(t)$ by $\hat{K}^j(b)(t)$, $j \geq 1$ through

$$\begin{aligned} \hat{K}(b)(t) &= \frac{1}{n} \sum_{i=1}^n [\hat{X}_i^{(q)}(t) - \bar{\hat{X}}^{(q)}(t)] (Y_i - \bar{Y}) \\ \hat{K}^2(b)(t) &= \int_{\mathcal{I}} \hat{K}(b)(s) \hat{K}(s, t) ds \\ \hat{K}^{j+1}(b)(t) &= \int_{\mathcal{I}} \hat{K}^j(b)(s) \hat{K}(s, t) ds, \quad j = 1, 2, \dots, \end{aligned}$$

where $\bar{\hat{X}}^{(q)}(t) = \sum_{i=1}^n \hat{X}_i^{(q)}(t)/n$ and $\hat{K}(s, t)$ is estimated by (3.14). Then we obtain the orthonormal basis $\psi_j, j = 1, \dots$. Next we estimate β_j 's by solving (3.4). Denote the estimates obtained for β_1, \dots, β_p by $\hat{\beta}_1, \dots, \hat{\beta}_p$, then the final estimate for b_p is

$$\hat{b}_p = \sum_{j=1}^p \hat{\beta}_j \hat{\psi}_j. \quad (3.18)$$

It is worthwhile to mention that, in fitting the linear model (3.1), one can directly estimate the intensity functions by the kernel method (Diggle, 1985) and compute an empirical estimate of the covariance function by using the log of the estimated intensity functions. Then, the coefficient function b can be estimated through applying the functional principal component regression or partial least squares and by incorporating the estimated log-intensities and the covariance

functions. More detailed explanation is given in Section 4. Our simulation studies in Section 4 show the superiority of the P^3LS method in prediction of the response in comparison to these methods. This is due to incorporating the properties of the log-Gaussian Cox process in estimation of the log-intensities and the covariance function of the underlying Gaussian process.

Lastly, sometimes in practice, the set of event times (e.g. detection times in our motivating study) is not recorded, instead, total counts within subintervals are available for analysis. More precisely, for the point process Φ_i , one might only observe $N_i(B_j), j = 1, \dots, J$ over the partition $\{B_1, \dots, B_J\}$ of the time interval \mathcal{I} and not the event times $\{S_{i1}, S_{i2}, \dots\}$. In this case, when the intensity function is smooth and subintervals B_j are narrow enough so that the intensity is approximately constant over B_j , one can invoke to the properties of the homogeneous Poisson point processes that conditional on the number of points observed within an interval, unordered locations of points are independent and distributed uniformly over the interval (Parzen, 1999, Theorem 4A). Thus, within each subinterval $B_j, j = 1, \dots, J$ one can generate $N_i(B_j)$ realizations of a uniform random variable over B_j , say $S_{(i,j)} = \{S_{i,j,1}, \dots, S_{i,j,N_i(B_j)}\}, j = 1, \dots, J$ and form $\Phi_i = S_{(i,1)} \cup S_{(i,2)} \cup \dots \cup S_{(i,J)}$. This type of data is referred as histogram data (Streit and Streit, 2010).

4. SIMULATION

In this section we illustrate the performance of the P^3LS algorithm in estimation of the coefficient function as well as in prediction. We compare the proposed method with alternative functional regression methods as well as other intuitively-based sensible estimation procedures, as explained below. The motivation for exploring alternative methods is as follows: latent log-intensity functions can be estimated using smoothing techniques, such as the kernel method. Furthermore, the covariance function of the log-intensities can be estimated by calculating the sample covariance of the estimated log-intensity functions.

4.1 Alternative Methods

In addition to the P^3LS procedure, we consider the following methods for estimation of the coefficient function b .

- *Functional Principal Component Regression (FPCR)*: In order to estimate the coefficient function in (3.1), one can apply the functional principal component regression method to the estimated log-intensities. Here we estimate the log-intensities by an application of the kernel smoothing method (Diggle, 1985), i.e. given a point process Φ_i , the intensity function of the process is denoted by $\tilde{\lambda}_i(t)$ and estimated as

$$\tilde{\lambda}_i(t) = \sum_{x \in \Phi_i} \frac{\kappa_h(x-t)}{a(t;h)}, \quad (4.19)$$

where $\kappa(\cdot)$ is a kernel function, $\kappa_h(u) = \kappa(u/h)/h$, and $a(s;h) = \int \kappa_h(s-x)dx$ is an edge correction term.

- *Kernel PLS (KPLS)*: One can initially estimate the log-intensities $\log[\lambda_i(t)]$, $i = 1, \dots, n$ by $\tilde{X}_i = \log[\tilde{\lambda}_i(t)]$, where $\tilde{\lambda}_i(t)$ is estimated as in (4.19), and use it to estimate the covariance function $K(\cdot, \cdot)$, denoted as $\tilde{K}(\cdot, \cdot)$, by

$$\tilde{K}(s,t) = \frac{1}{n} \sum_{i=1}^n \left(\tilde{X}_i(s) - \bar{\tilde{X}}_i(s) \right) \left(\tilde{X}_i(t) - \bar{\tilde{X}}_i(t) \right), \quad (4.20)$$

where $\bar{\tilde{X}}(t) = \sum_{j=1}^n \tilde{X}_j(t)/n$. Then, the Functional PLS method of Delaigle and Hall (2012), described in Section 3, can be applied to the estimated log-intensities with the covariance function estimated by (4.20). This will be referred to as *KPLS*.

4.2 Simulation Results

In the simulation studies, we generated 200 realizations of the following random log-intensity functions.

$$\log(\lambda_{nobs}) = \sum_{j=1}^{20} \left(\frac{1}{\eta} \omega_j^{(nobs)} + 2.8 \right) \phi_j, \quad (4.21)$$

where $\eta = 10$, ϕ_1, \dots, ϕ_{20} are B-spline basis functions, and

$$\begin{aligned}\omega_1^{(nobs)} &= 0, \\ \omega_2^{(nobs)}, \omega_7^{(nobs)}, \omega_{13}^{(nobs)}, \omega_{18}^{(nobs)} &\stackrel{iid}{\sim} N(6, 1^2), \\ \omega_3^{(nobs)}, \omega_6^{(nobs)}, \omega_{14}^{(nobs)}, \omega_{17}^{(nobs)} &\stackrel{iid}{\sim} N(12, 4^2) \\ \omega_4^{(nobs)}, \omega_5^{(nobs)}, \omega_{15}^{(nobs)}, \omega_{16}^{(nobs)} &\stackrel{iid}{\sim} N(24, 8^2), \\ \omega_8^{(nobs)}, \omega_9^{(nobs)}, \omega_{10}^{(nobs)}, \omega_{11}^{(nobs)}, \omega_{12}^{(nobs)}, \omega_{19}^{(nobs)}, \omega_{20}^{(nobs)} &\stackrel{iid}{\sim} N(4, 1^2).\end{aligned}$$

In addition, we considered

$$b = \sum_{k=j}^{20} \vartheta_j \phi_j,$$

for the following three cases of the coefficients $\vartheta_1, \dots, \vartheta_{20}$:

- Case 1: $\vartheta_j = \mathbb{I}\{2 \leq j \leq 7\}$, $j = 1, \dots, 20$.
- Case 2: $\vartheta_j = \mathbb{I}\{9 \leq j \leq 14\} + (-1) \times \mathbb{I}\{15 \leq j \leq 20\}$, $j = 1, \dots, 20$.
- Case 3: $\vartheta_j = (-1)^j \mathbb{I}\{2 \leq j \leq 6\} + (-1)^{j+1} \mathbb{I}\{15 \leq j \leq 19\}$, $j = 1, \dots, 20$.

Then, y_1, \dots, y_{200} were generated according to the model (3.1) with $a = 0$ and $\epsilon_i \stackrel{iid}{\sim} N(0, 1)$. In construction of the coefficient functions we considered examples of a functional relationship where, in Case 1, the response is highly correlated with an integrated log-intensity (or equivalently with photon counts) over a short period of time; in Case 2, the response is highly correlated with a contrast in the log-intensity over two periods of time; and in Case 3, the response is highly correlated with an oscillatory contrast in the log-intensity spanning over several periods of time. Plots of the coefficient functions considered in Cases 1-3 are illustrated in Figure 2.

To make comparisons, we consider 200 realizations of a temporal Gaussian process generated from the corresponding log-Gaussian Cox process. The randomly selected $n = 100$ samples were used as a training set and another $n_t = 100$ samples as a testing set. The mean square estimation

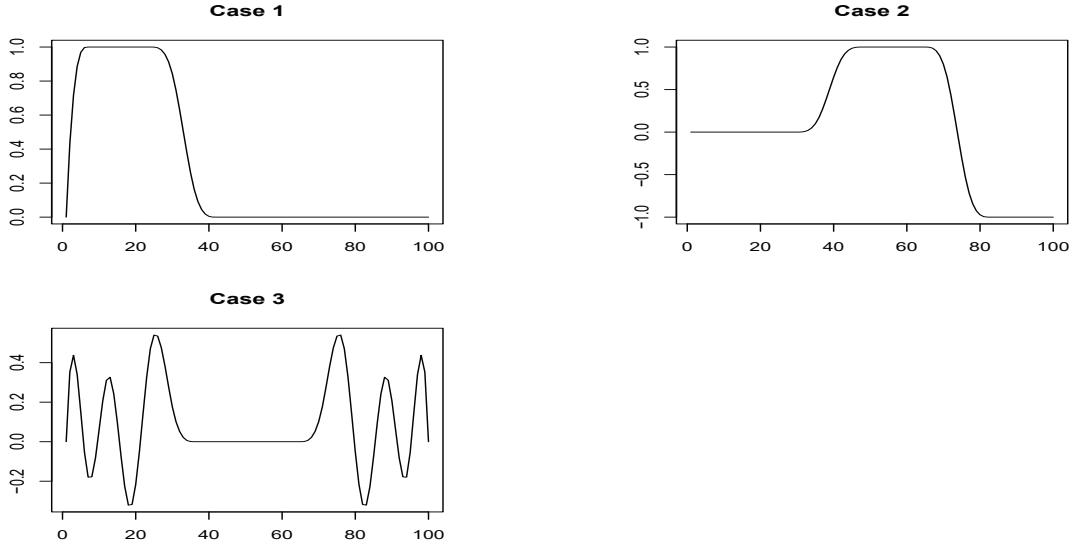


Fig. 2: Plots of the coefficient functions considered in Case 1 (**Top Panel**), Case 2 (**Middle Panel**), and Case 3 (**Bottom Panel**).

error (MSEE) of the coefficient function, is defined as

$$MSEE = \int_{\mathcal{I}} [b(t) - b_p(t)]^2 dt, \quad (4.22)$$

and the mean square prediction error ($MSPE$) of the testing responses, is defined as

$$MPSE = \frac{1}{n_t} \sum_{j=1}^{n_t} \left(y_j^{(test)} - \hat{y}_j^{(test)} \right)^2, \quad (4.23)$$

where $y_j^{(test)}$ and $\hat{y}_j^{(test)}$, $j = 1, \dots, n_t$ are the response values in the testing set and their predicted values, respectively. The data generation and model fitting procedure were repeated 100 times and boxplots of the root $MSEEs$ and root $MSPEs$ were computed for $p = 1, \dots, 10$ basis functions involved in estimation of the coefficient function.

Here we illustrate boxplots of the root $MSEE$ of the coefficient functions, in Figure 4, as well as the boxplots of the root $MSPE$ of the estimated model on the testing data set, in Figure 3, for $p = 1, \dots, 10$ basis functions, estimated by the P^3LS , $FPCR$, and $KPLS$. As Figure 3 illustrates, the P^3LS procedure has the least $MSPE$ compared to the other alternative methods

considered and also its performance is more stable over p . Regarding the $MSEE$ of estimation of the coefficient functions, as Figure 4 represents, all three methods achieve comparable $MSEE$ with small number of basis functions, however, $KPLS$ increases the $MSEE$ as p increases.

In conclusion, simulations show that smaller $MSPE$ can be achieved by the P^3LS method with smaller number of basis functions, comparing to the alternative functional or PLS methods considered in this paper, in addition that the prediction is more stable, while achieving $MSEE$ of smaller or of the same magnitude as the other methods.

5. DATA ANALYSIS

The data considered in this paper were collected from $N = 131$ patients, where scans of both kidneys were available for 122 of them and renogram data of only one kidney was available for 9 subjects, with data available for 127 left and 126 right kidneys. Of those 131 subjects, 66 were female and 65 were male with median age of 59 where 75% of them were between 48 to 70 years old. An expert interpreted the degree of obstruction for each kidney (rating score) ranging from -1.0 to 1.0 with higher scores indicating higher likelihood of obstruction and lower scores indicating no obstruction.

To generate renogram curves, the gamma camera recorded photon counts over 24 minutes in 59 frames for the baseline scan and 40 frames over 20 minutes in the diuretic scan as seen in Figure 1. Photon counts recorded are the total number of photons detected within the regions of interests over each framing time window. Since the observed counts within a frame is derived from a Poisson process, the data considered here can be treated as histogram data. Each dot on the curve in Figure 1 represents a total photon count within a frame. For example, if the photon count is 400 within a frame, we sample 400 time points that are uniformly distributed from starting time to the ending time of the frame, as described in Section 3.

In our analysis, we used data from 100 kidneys as training set and evaluated the trained model

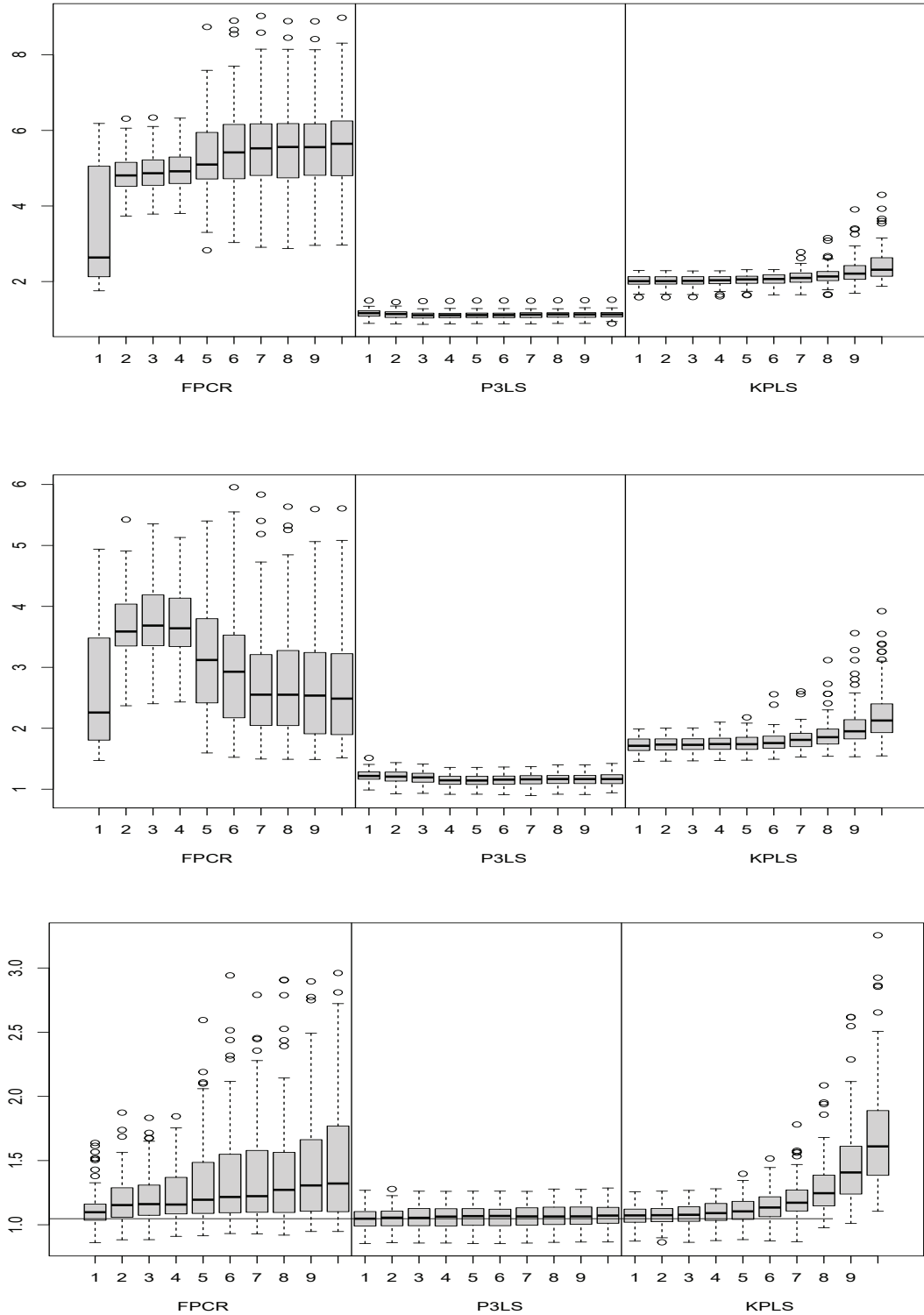


Fig. 3: **Top Panel:** Root $MSPE$ of Case 1, **Middle Panel:** Root $MSPE$ of Case 2, **Bottom Panel:** Root $MSPE$ of Case 3.

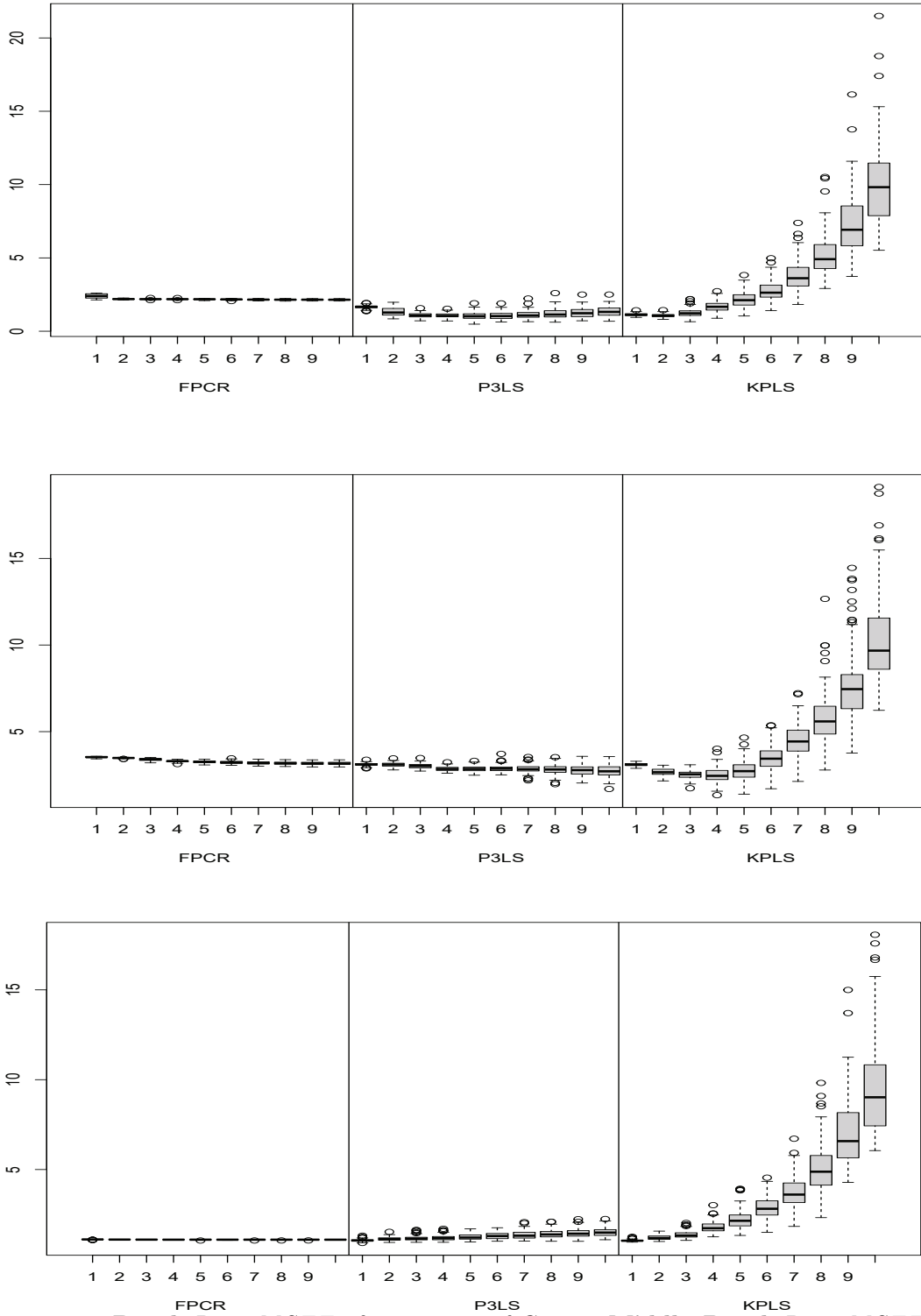


Fig. 4: **Top Panel:** Root $MSEE$ of estimation of Case 1, **Middle Panel:** Root $MSEE$ of estimation of Case 2, **Bottom Panel:** Root $MSEE$ of estimation of Case 3.

using the remaining data. We applied the point process PLS explained in Section 3 to the data from the left and right kidneys separately and in our analysis, we incorporated both the baseline and the diuretic photon counts. To do so, we concatenated the baseline and diuretic time series and considered it as a realization of an inhomogeneous Poisson point process. We then estimated the basis functions and the coefficient function of the predictive model (3.1) from the training data set. We chose two basis functions as suggested Bayesian Information Criteria.

Top panel of Figure (5) illustrates the estimated coefficient function of the predictive model (3.1) for both the left and right kidneys. For both kidneys, the estimated coefficient function is positive across all times for the diuretic renogram and negative across all times for the baseline renogram. It represents a contrast between diuretic and baseline renograms such that larger increases in diuretic log-intensities relative to baseline are associated with higher expected expert scores. This association is consistent with expert clinical knowledge, where larger values of the expert score are associated with obstruction and where the renogram curve of an obstructed kidney tends to increase during the baseline scan and stay at the same or higher level during the diuretic scan. This behavior is illustrated in the sample data displayed in Figure 1, where the renograms for kidneys with expert scores of -0.9 decrease from baseline to diuretic, while the renograms for the kidneys with the highest expert scores of -0.5 and 0.3 have constant or increased values.

The estimated two basis functions, which are displayed in the middle panel of Figure 5, also represent contrasts and provide insight into parsimonious temporal renogram information that is predictive of obstruction. The first basis function is negative for early baseline times before 9 minutes, and positive for both late baseline times after 9 minutes as well as for all diuretic times. This quantifies the common behavior of renograms of non-obstructed kidneys that increase, reaches its peak and declines gradually over baseline, then continues declining during diuretic, compared to the common behavior of obstructed kidneys that continues to increase. This behavior

is illustrated by the sample data displayed in Figure (5), where it peaks and declines during the baseline period in the subjects with expert scores of -0.9 compared to those with worse scores. The second basis function is positive at all baseline time points and negative at all diuretic time points, which provides a contrast that is consistent with the shape and level of the renogram curves. This aligns with established knowledge on renography interpretation and demonstrates that our model offers meaningful insights into interpreting kidney obstruction.

We also computed the $MSPE$ for the $FPCR$ method to illustrate the predictive superiority of the P^3LS compared with the commonly used methods of $FPCR$ for fitting the linear model (3.1). Bottom panel of Figure (5) illustrates that for any number $p = 1, \dots, 10$ of basis functions the P^3LS has smaller mean squared prediction error. Further more, the plot of $MSPE$ illustrates that two basis functions sufficiently explain the variation in the data, as it stabilizes when p increases. We also carried out the $KPLS$ method (results are not reported here) and the $KPLS$ had larger $MSPE$ than P^3LS , and increases as the number of basis functions increase as seen in the simulation studies. Finally, we have developed software to perform our method and examples are included to demonstrate its utility. See Web Appendix.

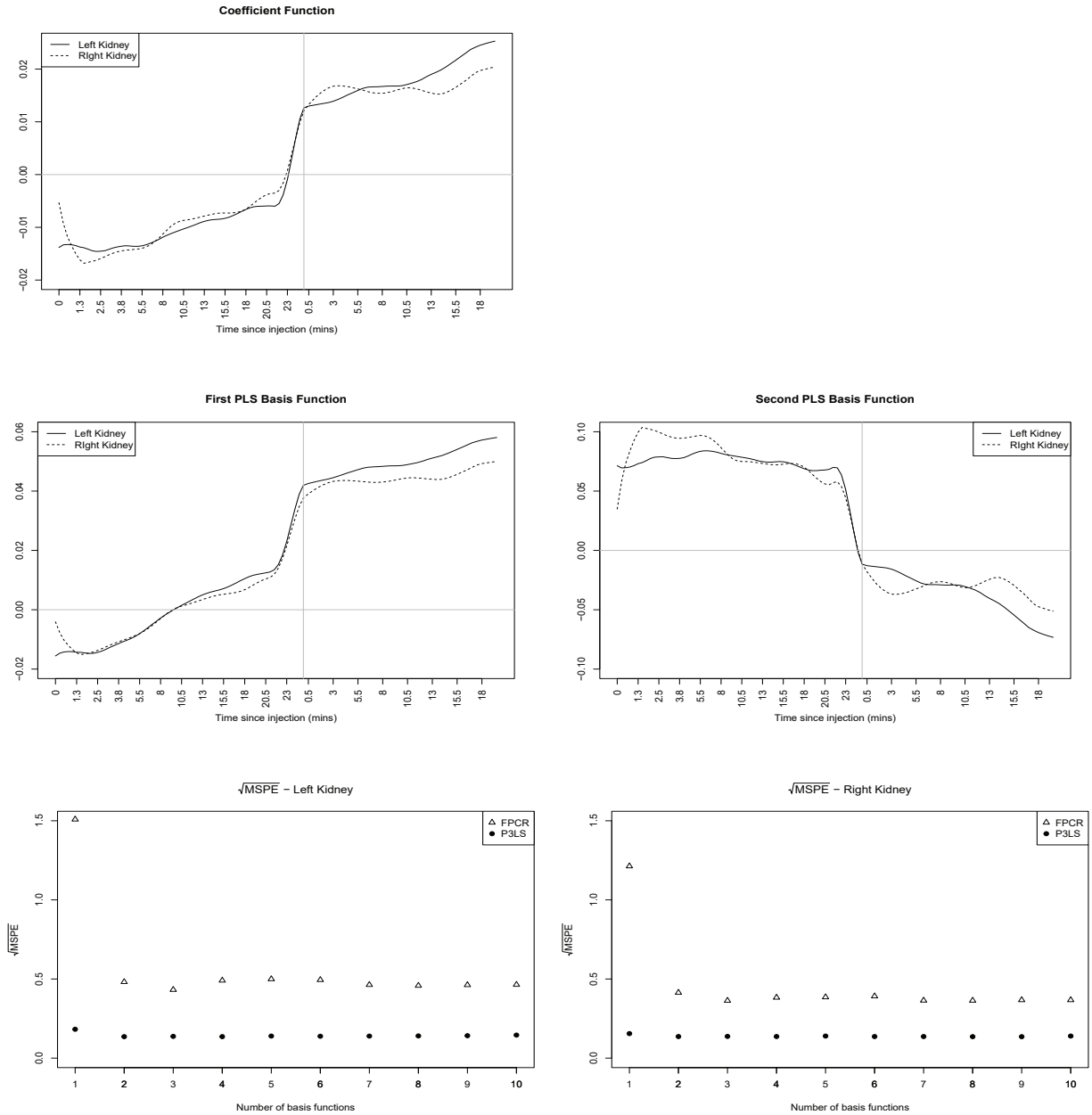


Fig. 5: **Top Left panel** The coefficient functions estimated for the left (solid line) and right (dashed line) kidneys. **Middle Left panel** The first PLS basis function of the left (solid line) and right (dashed line) kidney; **Middle right pane**: The second PLS basis function of the left (solid line) and right (dashed line) kidney. **Bottom left panel** Root $MSPE$ of the left kidney obtained by FPCR (triangle) and P^3LS (dot); **Bottom right pane**: Root $MSPE$ of the right kidney obtained by FPCR (triangle) and P^3LS (dot).

6. DISCUSSION

This article introduced, to the best of our knowledge, the first extension of partial least squares to point process data. We have explored its performance in comparison with some intuitive approaches to linear prediction with point process covariates in various settings of practical interest. We believe that the superiority of the method over the alternative approaches to linear prediction with log-Gaussian Cox processes as covariates stems from incorporation of the properties of the process in estimation of the covariance function as well as the log-intensity functions. This has motivated us to investigate the theoretical properties of the P^3LS , and in particular to determine precisely the class of functions where all combinations of the coefficient functions and log-intensities result in a smaller $MSPE$ comparing to $FPCR$, which will be reported elsewhere. The method is not exhaustive and can be extended to more complicated scenarios. In our motivating study, we analyzed the left and right kidneys separately, despite the fact that the data contains scans of both kidneys for 122 of the patients. An optimal analysis of the data needs to account for the dependence within and between the levels in a multilevel data, where an extension of the PLS is needed. The second extension is to incorporate space-time point processes. In many medical image studies in nuclear medicine, two dimensional images are produced using gamma camera for each subject. Extension of the method to higher dimensional point processes can potentially be of interest.

7. SOFTWARE

Software in the form of R codes, along with an example dataset, is attached to supplementary materials.

SUPPLEMENTARY MATERIAL

Contains the R-package “P3LS” and a pdf file containing modified Gram-Schmidt orthonormalization procedure.

ACKNOWLEDGMENTS

We thank Dr. Andrew Taylor at the department of nuclear medicine, Emory university, for informative discussions with the renal study.

FUNDING

This work is supported by National Institutes of Health grants R01GM140476, R01HL159213 and R01MH125816.

CONFLICT OF INTEREST STATEMENT

None declared.

REFERENCES

- ABDI, HERVÉ. (2010). Partial least squares regression and projection on latent structure regression (pls regression). *Wiley Interdisciplinary Reviews: Computational Statistics* **2**(1), 97–106.
- BAO, JIEQIONG, MANATUNGA, AMITA, BINONGO, JOSE NILO G AND TAYLOR, ANDREW T. (2011). Key variables for interpreting 99mTc-mercaptoacetyl triglycine diuretic scans: development and validation of a predictive model. *American Journal of Roentgenology* **197**(2), 325–333.
- CHANG, CHANGGEE, JANG, JEONG HOON, MANATUNGA, AMITA, TAYLOR, ANDREW T. AND

- LONG, QI. (2020). A bayesian latent class model to predict kidney obstruction in the absence of gold standard. *Journal of the American Statistical Association* **115**(532), 1645–1663.
- DALEY, DARYL J. AND VERE-JONES, DAVID. (2003). *An Introduction to the Theory of Point Processes*, Volume I: Elementary Theory and Methods. Springer.
- DELAIGLE, AURORE AND HALL, PETER. (2012). Methodology and theory for partial least squares applied to functional data. *The Annals of Statistics* **40**(1), 322–352.
- DIGGLE, PETER. (1985). A kernel method for smoothing point process data. *Journal of the Royal Statistical Society: Series C (Applied Statistics)* **34**(2), 138–147.
- JAKSIĆ, E, BEATOVIĆ, S, PAUNKOVIĆ, N, STEFANOVIĆ, A AND HAN, R. (2005). Variability in interpretation of static renal scintigraphy findings. *Vojnosanitetski Pregled* **62**(3), 189–193.
- KRISHNAN, ANJALI, WILLIAMS, LYNNE J, MCINTOSH, ANTHONY RANDAL AND ABDI, HERVÉ. (2011). Partial least squares (pls) methods for neuroimaging: a tutorial and review. *Neuroimage* **56**(2), 455–475.
- MØLLER, JESPER, SYVERSVEN, ANNE RANDI AND WAAGEPETERSEN, RASMUS PLENGE. (1998). Log gaussian cox processes. *Scandinavian Journal of Statistics* **25**(3), 451–482.
- O'REILLY, PATRICK, AURELL, MATTIUS, BRITTON, KEITH, KLETTER, KLAUS, ROSENTHAL, LEONARD AND TESTA, TITO. (1996). Consensus on diuresis renography for investigating the dilated upper urinary tract. *Journal of Nuclear Medicine* **37**(11), 1872–1876.
- PARZEN, EMANUEL. (1999). *Stochastic Processes*. SIAM.
- RAMSAY, JAMES O. AND SILVERMAN, BERNARD. (2005). *Functional Data Analysis*. Springer.
- ROSIPAL, ROMAN AND KRÄMER, NICOLE. (2005). Overview and recent advances in partial least squares. In: *International Statistical and Optimization Perspectives Workshop "Subspace, Latent Structure and Feature Selection"*. Springer. pp. 34–51.

- STREIT, ROY L AND STREIT, ROY L. (2010). *The Poisson Point Process*. Springer.
- TAYLOR, ANDREW, GARCIA, ERNEST V., BINONGO, JOSE NILO G., MANATUNGA, AMITA, HALKAR, RAGHUVeer, FOLKS, RUSSELL D. AND DUBOVSKY, EVA. (2008). Diagnostic performance of an expert system for interpretation of 99mTc mag3 scans in suspected renal obstruction. *Journal of Nuclear Medicine* **49**(2), 216–224.
- TAYLOR, ANDREW T., BLAUFOX, M. DONALD, DE PALMA, DIEGO, DUBOVSKY, EVA V., ERBAŞ, BELKIS, ESKILD-JENSEN, ANNI, FRØKIÆR, JØRGEN, ISSA, MUTA M., PIEPSZ, AMY AND PRIGENT, ALAIN. (2012). Guidance document for structured reporting of diuresis renography. *Seminars in Nuclear Medicine* **42**(1), 41–48. Planar Imaging in the Age of SPECT.
- WOLD, HERMAN. (1966). Estimation of principal components and related models by iterative least squares. *Journal of Multivariate Analysis*, 391–420.
- XU, GANGGANG, WANG, MING, BIAN, JIANGZE, HUANG, HUI, BURCH, TIMOTHY R, ANDRADE, SANDRO C, ZHANG, JINGFEI AND GUAN, YONGTAO. (2020). Semi-parametric learning of structured temporal point processes. *Journal of Machine Learning Research* **21**(192), 1–39.

P³LS: Point Process Partial Least Squares Supplementary Materials

Jamshid Namdari*, Robert T. Krafty, Amita Manatunga

Department of Biostatistics & Bioinformatics, Emory University, Atlanta, GA, United States

E-mail: jamshid.namdari@emory.edu

1. MODIFIED GRAM-SCHMIDT ALGORITHM

This algorithm constructs a set of unit length orthogonal basis functions u_1, \dots, u_p from a set of linearly independent functions v_1, \dots, v_p , where orthogonality is defined with respect to the inner product $\langle \cdot, \cdot \rangle$. For two functions f_1 and f_2 , the inner product is defined as

$$\langle f_1, f_2 \rangle = \int_{\mathcal{I}} \int_{\mathcal{I}} f_1(s) K(s, t) f_2(t) ds dt, \quad (1.1)$$

where $K(\cdot, \cdot)$ is a kernel function. The modified Gram-Schmidt algorithm is as follows:

Algorithm 1: Modified Gram-Schmidt

Input: Set of linearly independent functions v_1, \dots, v_p

Output: Set of orthogonal functions u_1, \dots, u_p

for $j \in \{1, \dots, p\}$ **do**

$$u_j^{[1]} = v_j$$

$$\text{For } i = 1, \dots, j - 1 \quad u_j^{[i+1]} = u_j^{[i]} - \langle u_j^{[i]}, u_i \rangle u_i$$

$$u_j = u_j^{[j]} / \|u_j^{[j]}\|$$

end

Output: u_1, \dots, u_p

*To whom correspondence should be addressed.